JOURNAL OF GUIDANCE, CONTROL, AND DYNAMICS
Vol. 32, No. 3, May–June 2009

Fuel-Optimal Maneuvers for Constrained Relative Satellite Orbits

David J. Irvin Jr.* and Richard G. Cobb†
Air Force Institute of Technology, Dayton, Ohio 45433
and
T. Alan Lovell‡
U.S. Air Force Research Laboratory, Albuquerque, New Mexico 87117

DOI: 10.2514/1.36618

This research investigates strategies to enable a deputy satellite to hover within a defined volume fixed in the vicinity of a chief satellite in a circular orbit for an extended period of time. Previous research developed initial methodologies for maintaining restricted teardrop hover orbits that exist in a plane fixed within the chief's local reference frame. These methods use the natural drift of the deputy satellite in the relative frame and impulsive thrust to keep the deputy in a bounded volume relative to the chief, but do not address fuel optimality. This research extends and enhances that work by finding the optimal trajectories produced with discrete thrusts that minimize fuel spent per unit time and stay within the user-defined volume, thus providing a practical hover capability in the vicinity of the chief. The work assumes that the Clohessy–Wiltshire closeness assumption between the deputy and chief is valid. Using the new methodology developed in this work, feasible closed- and nonclosed-relative orbits are found and evaluated based on a fuel criterion and are compared with an easily calculated continuous-thrust baseline. It is shown that in certain scenarios (generally corresponding to a smaller total time of flight) a discrete-thrust solution provides a lower overall fuel cost than a continuous-thrust solution. A simple check is proposed that enables the mission planner to make the correct strategy choice.

Nomenclature

a	=	chief orbit semimajor axis
h	=	half-height of the lobe in the cross-track dimension
J	=	value of the cost function
n	=	chief orbit mean motion
P	=	chief orbit period
T	=	time of flight
t	=	time
v	=	relative velocity
α	=	angular position of the lobe center in the $\hat{\mathbf{X}}$ $\hat{\mathbf{Y}}$ plane
β	=	angular position of the lobe center with respect to the $\hat{\mathbf{Z}}$ axis
γ	=	distance from chief to lobe center
ΔV	=	instantaneous change in velocity
$\Delta \check{V}$	=	specific delta V (ratio of ΔV to n)
η	=	angular orientation of the lobe in the $\hat{\mathbf{X}}$ $\hat{\mathbf{Y}}$ plane
μ	=	gravitational parameter (two body)
τ_x, τ_y	=	semimajor/minor axes of lobe
ψ	=	angular position on the lobe boundary

Subscripts

L	=	lobe center
XY	=	$\hat{\mathbf{X}}$ $\hat{\mathbf{Y}}$ plane
TD	=	teardrop
C	=	continuous
T	=	total
o	=	initial
f	=	final
z	=	in the $\hat{\mathbf{Z}}$ direction

Superscripts

$\hat{}$	=	chief centered reference frame
$\tilde{}$	=	denotes that time is expressed in chief orbit fractions

Presented as Paper 271 at the 2007 AAS-AIAA Astrodynamics Specialist Conference, Mackinac Island, MI, 19–23 August 2007; received 11 January 2008; revision received 5 December 2008; accepted for publication 5 December 2008.

*Ph.D. Graduate, Department of Aeronautics & Astronautics. Senior Member AIAA.
†Assistant Professor, Department of Aeronautics & Astronautics. Associate Fellow AIAA.
‡Research Engineer, Space Vehicles Directorate. Senior Member AIAA.

I. Introduction

SATELLITE formation flying and proximity operations have seen significant research interest in recent years. Advances have supported a host of capabilities that will be essential for maintaining critical space systems in the 21st century, including repairing, refueling, upgrading, augmenting, and otherwise servicing on-orbit assets. A related but less mature type of close-proximity operation is the ability to "hover" in a specific zone relative to the target satellite. A deputy satellite with the ability to hover could engage in monitoring or inspection missions. Hover capability has been demonstrated in a few constrained cases and in missions about smaller planetary bodies such as asteroids [1,2]. The goal of this research is to extend the hover capability within an arbitrarily placed volume fixed in the target satellite's local area. Note that, because these trajectories will, in general, not be on a single naturally drifting relative orbit, thrusting will be required. To best use limited fuel resources, we will focus on maximizing hovering time for a given amount of ΔV and, in doing so, address the feasibility of a variety of potential scenarios under consideration by mission planners. For the purposes of this research, the target satellite of interest, which is located at the center of the relative frame, will be called the "chief" satellite and the satellite operating in proximity to the chief will be called the "deputy." The problem can be stated as follows: *to develop a control strategy to place a deputy satellite inside a specific lobe defined in the chief body-fixed frame and keep it there in a fuel-optimal manner*. The control strategy proposed is to execute a series of impulsive thrusts such that the location, magnitude, and direction of thrust are the result of an optimization algorithm developed herein.

The simplest realizable case is the one in which two satellites share the same circular orbit but have different angular positions in their inertial orbits about the central body. In the absence of perturbations, the two would stay in a fixed relative position with each other. More flexibility is desired in the relative placement; thus, we seek to define a general closed volume of arbitrary size, location, and orientation near the chief satellite and fixed in the relative frame that bounds the relative motion of the deputy. A continuous-thrust solution is derived and used as a benchmark to compare to the resultant discrete-thrust trajectories. It should be noted that a continuous-thrust controller is a feasible control strategy for hovering satellites. Results are presented, however, that will demonstrate scenarios for which discrete-thrust solutions require less fuel. There may also be mission-related reasons for choosing a discrete-thrust strategy, such as limitations of the thruster or a desire to avoid plume impingement on the chief.

Previous work on hovering has considered closed orbits in the inertial plane of the chief satellite [3,4]. The teardrop orbit is designed by finding a drifting orbit in the relative frame that intersects itself, providing a point at which to perform a single impulsive thrust to keep the deputy in a constrained area. A more general framework for finding hovering orbits is proposed. We start with a discussion of relative dynamics followed by the development of a cost function and constraint. The paper presents results for several lobe entry and exit conditions as well as a discussion of special cases and concludes with a criterion on which to base a strategy decision.

II. Relative Motion Modeling

The relative motion of the deputy satellite with respect to the chief is modeled in the local-vertical/local-horizon (LVLH) frame. The $\hat{\mathbf{X}}$ (radial) axis is oriented along a line from the center of the Earth to the chief, the $\hat{\mathbf{Z}}$ (cross-track) axis is perpendicular to the orbit plane of the chief, and the $\hat{\mathbf{Y}}$ (in-track) axis completes the frame as the cross product $\hat{\mathbf{Z}} \times \hat{\mathbf{X}}$. The in-track direction is aligned with the velocity vector of the chief when in a circular orbit. Assume the chief satellite is in a circular orbit and the gravity of the central body is the only force of significance. The equations of relative motion are [5]

$$\ddot{x} - 2n\dot{y} - n^2(x+a)\left[1 - \frac{a^3(x+a)}{[(x+a)^2 + y^2 + z^2]^{\frac{3}{2}}}\right] = 0 \tag{1a}$$

$$\ddot{y} + 2n\dot{x} - n^2 y\left[1 - \frac{a^3}{[(x+a)^2 + y^2 + z^2]^{\frac{3}{2}}}\right] = 0 \tag{1b}$$

$$\ddot{z} + n^2 z\left[\frac{a^3}{[(x+a)^2 + y^2 + z^2]^{\frac{3}{2}}}\right] = 0 \tag{1c}$$

where a is the semimajor axis of the chief and n is the mean motion. If we assume that the deputy is close to the chief satellite in comparison to the chief's semimajor axis,

$$\sqrt{x^2 + y^2 + z^2} \ll a$$

then the relative equations reduce to

$$\ddot{x} - 2n\dot{y} - 3n^2 x = 0 \tag{2a}$$

$$\ddot{y} + 2n\dot{x} = 0 \tag{2b}$$

$$\ddot{z} + n^2 z = 0 \tag{2c}$$

It is possible, and highly desirable for this application, to express time as a fraction of the chief orbit period (P) as opposed to an absolute time. The relative equations can now be written independent of a particular semimajor axis and gravitational parameter (μ). Let [6]

$$\tilde{t} = t/P = (n/2\pi)t \tag{3}$$

Expressing time in chief orbit periods will scale the relative velocity and acceleration but not the relative position; thus,

$$\tilde{x} = x, \qquad \tilde{y} = y, \qquad \tilde{z} = z \tag{4}$$

The derivative of t with respect to $\tilde{t}$ is

$$\frac{\mathrm{d}t}{\mathrm{d}\tilde{t}} = \frac{2\pi}{n} \tag{5}$$

Leading to the following relationship of relative velocity:

$$\dot{\tilde{x}} = \frac{\mathrm{d}\tilde{x}}{\mathrm{d}\tilde{t}} = \frac{\mathrm{d}x}{\mathrm{d}\tilde{t}} = \frac{\mathrm{d}x}{\mathrm{d}t}\frac{\mathrm{d}t}{\mathrm{d}\tilde{t}} = \dot{x}\frac{2\pi}{n} \tag{6}$$

and likewise for $\dot{\tilde{y}}$ and $\dot{\tilde{z}}$. For the relative accelerations,

$$\ddot{\tilde{x}} = \frac{\mathrm{d}\dot{\tilde{x}}}{\mathrm{d}\tilde{t}} = \frac{2\pi}{n}\frac{\mathrm{d}\dot{x}}{\mathrm{d}\tilde{t}} = \frac{2\pi}{n}\frac{\mathrm{d}\dot{x}}{\mathrm{d}t}\frac{\mathrm{d}t}{\mathrm{d}\tilde{t}} = \ddot{x}\frac{4\pi^2}{n^2} \tag{7}$$

Applying these relationships to Eq. (2),

$$\ddot{\tilde{x}} - 4\pi\dot{\tilde{y}} - 12\pi^2\tilde{x} = 0 \tag{8a}$$

$$\ddot{\tilde{y}} + 4\pi\dot{\tilde{x}} = 0 \tag{8b}$$

$$\ddot{\tilde{z}} + 4\pi^2\tilde{z} = 0 \tag{8c}$$

the solution to which is [7]

$$\tilde{x}(\tilde{t}) = \frac{1}{2\pi}\dot{\tilde{x}}_o \sin(2\pi\tilde{t}) - \left[\frac{1}{\pi}\dot{\tilde{y}}_o + 3\tilde{x}_o\right]\cos(2\pi\tilde{t}) + \frac{1}{\pi}\dot{\tilde{y}}_o + 4\tilde{x}_o \tag{9a}$$

$$\tilde{y}(\tilde{t}) = \left[\frac{2}{\pi}\dot{\tilde{y}}_o + 6\tilde{x}_o\right]\sin(2\pi\tilde{t}) + \frac{1}{\pi}\dot{\tilde{x}}_o\cos(2\pi\tilde{t}) - [3\dot{\tilde{y}}_o + 12\pi\tilde{x}_o]\tilde{t} - \frac{1}{\pi}\dot{\tilde{x}}_o + \tilde{y}_o \tag{9b}$$

$$\tilde{z}(\tilde{t}) = \frac{1}{2\pi}\dot{\tilde{z}}_o \sin(2\pi\tilde{t}) + \tilde{z}_o\cos(2\pi\tilde{t}) \tag{9c}$$

$$\dot{\tilde{x}}(\tilde{t}) = \dot{\tilde{x}}_o\cos(2\pi\tilde{t}) + [2\dot{\tilde{y}}_o + 6\pi\tilde{x}_o]\sin(2\pi\tilde{t}) \tag{9d}$$

$$\dot{\tilde{y}}(\tilde{t}) = [4\dot{\tilde{y}}_o + 12\pi\tilde{x}_o]\cos(2\pi\tilde{t}) - 2\dot{\tilde{x}}_o\sin(2\pi\tilde{t}) - 3\dot{\tilde{y}}_o - 12\pi\tilde{x}_o \tag{9e}$$

$$\dot{\tilde{z}}(\tilde{t}) = \dot{\tilde{z}}_o\cos(2\pi\tilde{t}) - 2\pi\tilde{z}_o\sin(2\pi\tilde{t}) \tag{9f}$$

These linear time-invariant, constant coefficient, differential equations are the classical Clohessy–Wiltshire (CW) equations [8], albeit in a less conventional form. For this research, the most important information to extract from these equations are the initial and final relative velocities. They are key to calculating ΔV as well as initializing trajectory propagation to check for breaches of the lobe boundary. The initial relative velocity, under the circular chief orbit assumption, that will cause the deputy to move from $(\tilde{x}_o, \tilde{y}_o, \tilde{z}_o)$ to $(\tilde{x}_f, \tilde{y}_f, \tilde{z}_f)$ over the time period $\tilde{T}$ is [6,9]

$$\begin{bmatrix} \dot{\tilde{x}}_o \\ \dot{\tilde{y}}_o \\ \dot{\tilde{z}}_o \end{bmatrix} = 2\pi \begin{bmatrix} \frac{-4\tilde{S}+6\pi\tilde{T}\tilde{C}}{8-6\pi\tilde{T}\tilde{S}-8\tilde{C}} & 0 & \frac{4\tilde{S}-6\pi\tilde{T}}{8-6\pi\tilde{T}\tilde{S}-8\tilde{C}} & 0 & \frac{-2+2\tilde{C}}{8-6\pi\tilde{T}\tilde{S}-8\tilde{C}} \\ \frac{-14+12\pi\tilde{T}\tilde{S}+14\tilde{C}}{8-6\pi\tilde{T}\tilde{S}-8\tilde{C}} & 0 & \frac{2-2\tilde{C}}{8-6\pi\tilde{T}\tilde{S}-8\tilde{C}} & 0 & \frac{\tilde{S}}{8-6\pi\tilde{T}\tilde{S}-8\tilde{C}} \\ 0 & -\frac{\tilde{C}}{\tilde{S}} & 0 & \frac{1}{\tilde{S}} & 0 \end{bmatrix} \begin{bmatrix} \tilde{x}_o \\ \tilde{z}_o \\ \tilde{x}_f \\ \tilde{z}_f \\ \Delta\tilde{y} \end{bmatrix} \tag{10}$$

where $\tilde{T} = T/P$, $\tilde{S} = \sin(2\pi\tilde{T})$, $\tilde{C} = \cos(2\pi\tilde{T})$, and $\Delta\tilde{y} = \tilde{y}_f - \tilde{y}_o$. The final relative velocity is

$$\begin{bmatrix} \dot{\tilde{x}}_f \\ \dot{\tilde{y}}_f \\ \dot{\tilde{z}}_f \end{bmatrix} = 2\pi \begin{bmatrix} \frac{-4\tilde{S}+6\pi\tilde{T}}{8-6\pi\tilde{T}\tilde{S}-8\tilde{C}} & 0 & \frac{4\tilde{S}-6\pi\tilde{T}\tilde{C}}{8-6\pi\tilde{T}\tilde{S}-8\tilde{C}} & 0 & \frac{2-2\tilde{C}}{8-6\pi\tilde{T}\tilde{S}-8\tilde{C}} \\ \frac{2-2\tilde{C}}{8-6\pi\tilde{T}\tilde{S}-8\tilde{C}} & 0 & \frac{-14+12\pi\tilde{T}\tilde{S}+14\tilde{C}}{8-6\pi\tilde{T}\tilde{S}-8\tilde{C}} & 0 & \frac{\tilde{S}}{8-6\pi\tilde{T}\tilde{S}-8\tilde{C}} \\ 0 & -\frac{1}{\tilde{S}} & 0 & \frac{\tilde{C}}{\tilde{S}} & 0 \end{bmatrix} \begin{bmatrix} \tilde{x}_o \\ \tilde{z}_o \\ \tilde{x}_f \\ \tilde{z}_f \\ \Delta\tilde{y} \end{bmatrix} \tag{11}$$

Equation (8) also provides the means to calculate the ΔV costs for stationary hovering, which will be used later as a benchmark to compare our optimal trajectories. Note that stationary hovering requires the continuous application of thrust. To hover at a fixed point in the LVLH frame, the relative velocities are zero:

$$\dot{\tilde{x}} = 0 \qquad \dot{\tilde{y}} = 0 \qquad \dot{\tilde{z}} = 0 \tag{12}$$

which reduces Eq. (8) to

$$\ddot{\tilde{x}} = 12\pi^2\tilde{x} \qquad \ddot{\tilde{y}} = 0 \qquad \ddot{\tilde{z}} = -4\pi^2\tilde{z} \tag{13}$$

Because the $\ddot{\tilde{y}}$ equation is now zero, only accelerations in the $\hat{\mathbf{X}}$ and $\hat{\mathbf{Z}}$ directions are needed. Integrating from zero to the total time of flight ($\tilde{T}_T$) yields the ΔV as a function of the chief orbit period ($\Delta\tilde{V}_C$) required to keep the deputy hovering at a given $\tilde{x}_o$, $\tilde{y}_o$, and $\tilde{z}_o$:

$$\Delta\tilde{V}_C = \int_0^{\tilde{T}_T} |\ddot{\tilde{x}}|\,\mathrm{d}\tilde{t} + \int_0^{\tilde{T}_T} |\ddot{\tilde{z}}|\,\mathrm{d}\tilde{t} = \int_0^{\tilde{T}_T} 12\pi^2|\tilde{x}_o|\,\mathrm{d}\tilde{t} + \int_0^{\tilde{T}_T} 4\pi^2|\tilde{z}_o|\,\mathrm{d}\tilde{t} = \pi^2(12|\tilde{x}_o| + 4|\tilde{z}_o|)\int_0^{\tilde{T}_T} \mathrm{d}\tilde{t} = \pi^2(12|\tilde{x}_o| + 4|\tilde{z}_o|)\tilde{T}_T \tag{14}$$

where the subscript C represents "continuous" and the tilde indicates that the relative velocities are defined in terms of the chief orbit period. The location of $\tilde{x}_o$ and $\tilde{z}_o$ is arbitrary but, because ΔV is linear in position, the smallest continuous-thrust $\Delta\tilde{V}$ is attained when $\tilde{x}_o$ and $\tilde{z}_o$ are at their minimum [see Eq. (15)]. Note that this occurs at the point on the lobe that is closest to the $\hat{\mathbf{X}}\,\hat{\mathbf{Y}}$ plane and the $\hat{\mathbf{Y}}\,\hat{\mathbf{Z}}$ plane.

$$\Delta\tilde{V}_C = (12\tilde{x}_{\min} + 4\tilde{z}_{\min})\pi^2\tilde{T}_T \tag{15}$$

Finally, the relationship between ΔV and $\Delta\tilde{V}$ is found using Eq. (6):

$$\Delta V_i = \sqrt{(\dot{x}_i^+ - \dot{x}_i^-)^2 + (\dot{y}_i^+ - \dot{y}_i^-)^2} = \sqrt{(\frac{n}{2\pi}\dot{\tilde{x}}_i^+ - \frac{n}{2\pi}\dot{\tilde{x}}_i^-)^2 + (\frac{n}{2\pi}\dot{\tilde{y}}_i^+ - \frac{n}{2\pi}\dot{\tilde{y}}_i^-)^2} = \frac{n}{2\pi}\Delta\tilde{V}_i \tag{16}$$

With the equations of motion in hand, we next define the boundary volume that constrains the trajectory of the deputy. An ellipse is chosen in the chief's orbit plane (Fig. 1a), providing sufficient flexibility for designing hover regions without overly complicating the mathematics. The lobe size via τ_x and τ_y and the orientation via η is user defined. All thrusting is assumed to occur on the lobe boundary; thus, for a specific lobe those locations can be identified by a single coordinate, ψ. In the linearized equations of motion, the $\hat{\mathbf{Z}}$ direction is decoupled from motion in the $\hat{\mathbf{X}}\,\hat{\mathbf{Y}}$ plane; thus, an elliptical cylinder (Fig. 1b) is selected to prevent recoupling of those equations during the optimization [see Eq. (2)]. The lobe center is located a distance of γ away from the deputy.

$$x_L = \gamma_{XY}\cos\alpha = \gamma\cos\alpha\sin\beta$$
$$y_L = \gamma_{XY}\sin\alpha = \gamma\sin\alpha\sin\beta$$
$$z_L = \gamma\cos\beta$$

With the dynamics and trajectory boundaries defined, we seek a cost function that fulfills our objective to find fuel-optimal trajectories.

A. Cost Function

The problem statement suggests the use of an optimization problem and the formulation of a cost function. Because the in-plane and out-of-plane motion is decoupled in the linearized equations, they will be dealt with separately. Ideally, we want to maximize the time spent inside the lobe per unit of fuel expended or, equivalently, we can minimize the cost function (J):

$$J = \frac{\text{fuel spent}}{\text{time of flight}} = \frac{\sum_{i=1}^{k}\Delta V_i + \Delta V_f}{\sum_{i=1}^{k} T_{i,i+1} + T_f} \tag{17}$$

where k is the number of legs (a leg being defined as the trajectory between the ith and $[i+1]$th points), T is time of flight, and the subscript f represents a possible exit burn. All thrusting is assumed to occur on the lobe boundary. For the in-plane motion, the ΔV for each leg is calculated by taking the Euclidean norm of the difference between pre- and postthrust relative velocities (v):

$$\Delta V_i = \|\Delta\mathbf{v}_i\|_2 = \|\mathbf{v}_i^+ - \mathbf{v}_i^-\|_2 = \sqrt{(\dot{x}_i^+ - \dot{x}_i^-)^2 + (\dot{y}_i^+ - \dot{y}_i^-)^2} \tag{18}$$

Using ΔV^2 yields a more mathematically compact solution for impulsive thrust and allows for closed-form solutions of the cost function's gradient. Because ΔV is always positive, minimizing the square will minimize the value itself; thus, our expanded cost function is

$$J = \frac{\Delta V_1^2 + \Delta V_2^2 + \Delta V_3^2 + \cdots + \Delta V_k^2 + \Delta V_f^2}{T_{1,2} + T_{2,3} + T_{3,4} + \cdots + T_{k,k+1} + T_f} \tag{19}$$

As mentioned earlier, it is desirable to have equations that are not a function of the chief's semimajor axis or μ. To that end, the *specific* delta V ($\Delta\breve{V}$) is defined as

$$\Delta\breve{V} = \Delta V/n = \Delta\tilde{V}/2\pi \tag{20}$$

where the relationship between ΔV and $\Delta\tilde{V}$ is defined in Eq. (16). Using Eqs. (10) and (11), the square of $\Delta\breve{V}$ is

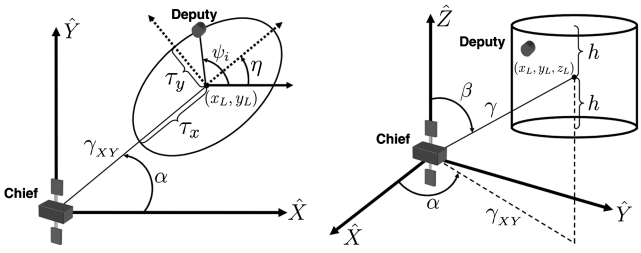

a) In-plane boundary **b) Out-of-plane boundary**

Fig. 1 Definition of the lobe parameters.

$$\Delta\check{V}_i^2 = [\,\tilde{x}_{i-1} \quad \tilde{y}_{i-1} \quad \tilde{x}_i \quad \tilde{y}_i \quad \tilde{x}_{i+1} \quad \tilde{y}_{i+1}\,]\tilde{R}\tilde{R}'\begin{bmatrix}\tilde{x}_{i-1}\\ \tilde{y}_{i-1}\\ \tilde{x}_i\\ \tilde{y}_i\\ \tilde{x}_{i+1}\\ \tilde{y}_{i+1}\end{bmatrix} \tag{21}$$

where $\tilde{R}$ is defined as

$$\tilde{R} = \begin{bmatrix} \frac{4\tilde{S}^- - 6\pi\tilde{T}^-}{8-6\pi\tilde{T}^-\tilde{S}^- - 8\tilde{C}^-} & \frac{-2+2\tilde{C}^-}{8-6\pi\tilde{T}^-\tilde{S}^- - 8\tilde{C}^-} \\ \frac{2-2\tilde{C}^-}{8-6\pi\tilde{T}^-\tilde{S}^- - 8\tilde{C}^-} & \frac{\tilde{S}^-}{8-6\pi\tilde{T}^-\tilde{S}^- - 8\tilde{C}^-} \\ \frac{-4\tilde{S}^+ + 6\pi\tilde{T}^+\tilde{C}^+}{8-6\pi\tilde{T}^+\tilde{S}^+ - 8\tilde{C}^+} - \frac{4\tilde{S}^- - 6\pi\tilde{T}^-\tilde{C}^-}{8-6\pi\tilde{T}^-\tilde{S}^- - 8\tilde{C}^-} & \frac{-14+12\pi\tilde{T}^+\tilde{S}^+ + 14\tilde{C}^+}{8-6\pi\tilde{T}^+\tilde{S}^+ - 8\tilde{C}^+} - \frac{-14+12\pi\tilde{T}^-\tilde{S}^- + 14\tilde{C}^-}{8-6\pi\tilde{T}^-\tilde{S}^- - 8\tilde{C}^-} \\ \frac{2-2\tilde{C}^+}{8-6\pi\tilde{T}^+\tilde{S}^+ - 8\tilde{C}^+} - \frac{2-2\tilde{C}^-}{8-6\pi\tilde{T}^-\tilde{S}^- - 8\tilde{C}^-} & \frac{-\tilde{S}^+}{8-6\pi\tilde{T}^+\tilde{S}^+ - 8\tilde{C}^+} - \frac{\tilde{S}^-}{8-6\pi\tilde{T}^-\tilde{S}^- - 8\tilde{C}^-} \\ \frac{4\tilde{S}^+ - 6\pi\tilde{T}^+}{8-6\pi\tilde{T}^+\tilde{S}^+ - 8\tilde{C}^+} & \frac{2-2\tilde{C}^+}{8-6\pi\tilde{T}^+\tilde{S}^+ - 8\tilde{C}^+} \\ \frac{-2+2\tilde{C}^+}{8-6\pi\tilde{T}^+\tilde{S}^+ - 8\tilde{C}^+} & \frac{\tilde{S}^+}{8-6\pi\tilde{T}^+\tilde{S}^+ - 8\tilde{C}^+} \end{bmatrix} \tag{22}$$

and $\tilde{T}^- = \tilde{T}_{i-1,i}$, $\tilde{T}^+ = \tilde{T}_{i,i+1}$, $\tilde{S}^- = \sin(2\pi\tilde{T}_{i-1,i})$, $\tilde{S}^+ = \sin(2\pi\tilde{T}_{i,i+1})$, $\tilde{C}^- = \cos(2\pi\tilde{T}_{i-1,i})$, and $\tilde{C}^+ = \cos(2\pi\tilde{T}_{i,i+1})$. Initial investigations into the problem found unacceptably flat cost functions, thus encouraging proper scaling. It is desirable to keep the numerator of Eq. (19) in the neighborhood of 1, which is accomplished by scaling by the continuous-thrust ΔV ($\Delta\check{V}_C$) in the $\hat{\mathbf{X}}\,\hat{\mathbf{Y}}$ plane required to keep the deputy at the $\tilde{x}_{\min}$ position (i.e., the point on the boundary closest to the $\hat{\mathbf{Y}}$ axis). Using Eqs. (15) and (20), the continuous-thrust ΔV is

$$\Delta\check{V}_C^2 = \left(\frac{\Delta\tilde{V}_C}{2\pi}\right)^2 = \left(\frac{12\pi^2\tilde{x}_{\min}\tilde{T}_T}{2\pi}\right)^2 = 36\pi^2\tilde{x}_{\min}^2\tilde{T}_T^2 \tag{23}$$

where $\tilde{T}_T$ is the total time of flight. Likewise, the time of flight is conveniently scaled by the chief's orbit period:

$$\begin{aligned}(1/P)[T_{1,2} + T_{2,3} + T_{3,4} + \cdots + T_{k,k+1} + T_f] \\ = \tilde{T}_{1,2} + \tilde{T}_{2,3} + \tilde{T}_{3,4} + \cdots + \tilde{T}_{k,k+1} + \tilde{T}_f\end{aligned} \tag{24}$$

Combining the scaling of ΔV and the time of flight, the cost function is now

$$J = \frac{\frac{1}{36\pi^2\tilde{x}_{\min}^2\tilde{T}_T^2}[\Delta\check{V}_1^2 + \Delta\check{V}_2^2 + \Delta\check{V}_3^2 + \cdots + \Delta\check{V}_k^2 + \Delta\check{V}_f^2]}{\tilde{T}_{1,2} + \tilde{T}_{2,3} + \tilde{T}_{3,4} + \cdots + \tilde{T}_{k,k+1} + \tilde{T}_f} \tag{25}$$

Note that the cost function is undefined when $\tilde{x}_{\min} = 0$. This implies that the lobe intersects the $\hat{\mathbf{Y}}$ axis, a special case of hovering orbits addressed in Sec. III.A.

B. Constraint

The trajectory of the deputy is completely defined for a given start and end position and transfer time of flight [see Eq. (9)]. Using Eq. (10) to find the initial relative velocity, an analysis of the effect of time of flight choice on relative trajectories is presented. All burns are assumed to occur on the lobe boundary; thus, their location on a specific lobe can be identified with a single coordinate (ψ). Given a start and end position, (ψ_1, ψ_2), a small time of flight produces a trajectory that closely approximates a straight line between the two points and has a large magnitude relative velocity. As the time of flight is increased, the trajectory exhibits larger and larger paths that may or may not cross back over themselves. As illustrated in Fig. 2, there is a maximum time of flight after which any larger time of flight creates a trajectory that partially leaves the constraint lobe. Figure 2 also demonstrates the "teardrop" or "pogo" maneuvers [3,4,10], that is a trajectory that intersects itself, providing the spacecraft an opportunity to perform a maneuver to keep itself on the looping path indefinitely.

From a mission planner's standpoint, the only constraint on the deputy satellite's motion is that it stays within the prescribed lobe. Although there are several methods to pose this constraint, the simplest one is to force the time of flight to be less than or equal to some maximum time of flight. This maximum time of flight is

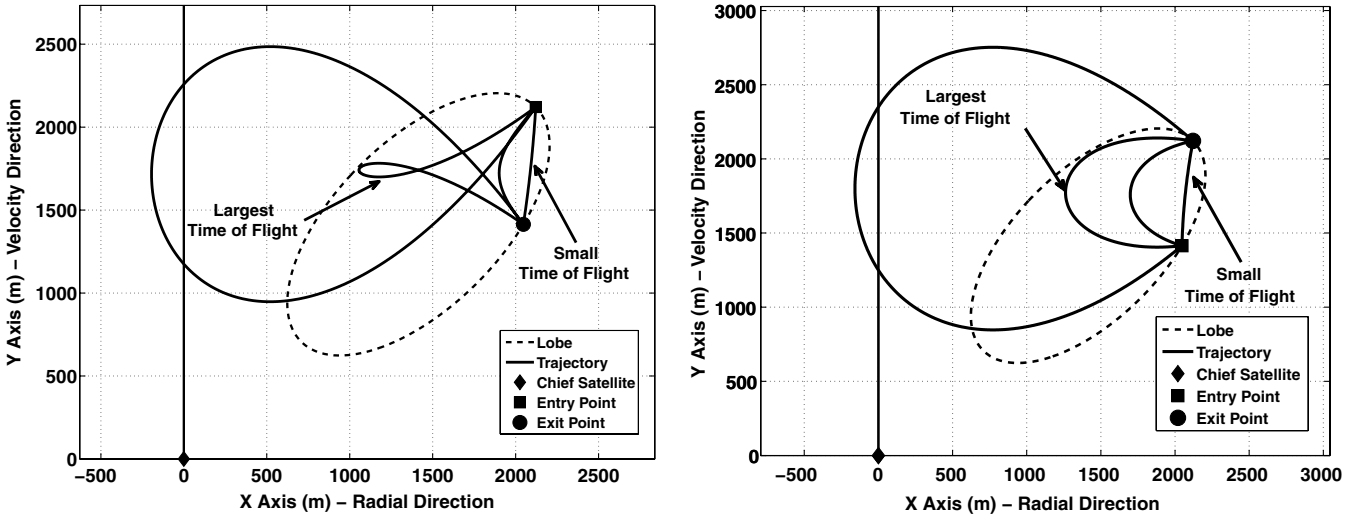

Fig. 2 Notional time of flight comparisons.

naturally defined as the largest time of flight for which the deputy's entire trajectory remains inside the lobe.

$$\tilde{T}_{i,i+1} \leq \tilde{T}_{\max_{i,i+1}}(\psi_1, \psi_2) \tag{26}$$

For this paper, the maximum time of flight is found using a bracketing search, evaluating the midpoint of the range until that range is less than 0.0005 chief orbit periods. Midpoints are evaluated by computing the trajectory for that time of flight to determine if the lobe boundary is breached. Using this method, a constraint surface is precomputable for a specific lobe size and position (example Fig. 3). Interpolating between points is a very effective way to calculate the constraint during optimization searches. All constraint surfaces have a valley of $\tilde{T}_{\max} = 0$, the set of ψ from which a trajectory cannot start and end without leaving the lobe no matter how small the time of flight. These points are located on the side of the lobe closest to the $\hat{\mathbf{Y}}$ axis. Because the lobe is a closed convex shape, we can always draw a straight line between any two points that stays completely within the lobe (and, as noted previously, as $\tilde{T} \to 0$ the trajectory becomes a straight line); therefore, this valley will always be along the line $\psi_1 = \psi_2$.

For motion along the $\hat{\mathbf{Z}}$ axis, it can be shown that the maximum time of flight for which the deputy stays between a minimum ($\tilde{z}_{\min}$) and maximum ($\tilde{z}_{\max}$) $\hat{\mathbf{Z}}$ coordinate is

$$\tilde{T}_{\max} = (1/\pi)\cos^{-1}(\tilde{z}_{\min}/\tilde{z}_{\max}) \tag{27}$$

A derivation is provided in the Appendix [see Eq. (A5)]. The $\cos^{-1}$ function has a domain of $0 < \tilde{z}_{\min}/\tilde{z}_{\max} < 1$, and this fits well with our definition of the elliptical cylinder. Motion in the $\hat{\mathbf{Z}}$ direction is caused by differences in the inclination and/or longitude of the ascending node between the chief and deputy. As intuition and Eq. (9c) indicate, the period of the $\hat{\mathbf{Z}}$ oscillation is 2π and is centered about the chief's orbit plane. Half the period is spent on one side of the chief's orbit plane and half on the other side. Thus, any $\hat{\mathbf{Z}}$ period greater than 0.5 would indicate that the deputy has passed through the chief's orbit plane. Lobes that include the chief's orbit plane will have $\tilde{z}_{\min}/\tilde{z}_{\max}$ ratios that are less than zero (change in sign between $\tilde{z}_{\min}$ and $\tilde{z}_{\max}$) and ill-defined lobes that are greater than 1 ($|\tilde{z}_{\min}|$ is larger than $|\tilde{z}_{\max}|$). Therefore, either the lobe intersects the orbit plane, in which case the optimal solution is to stay in the orbit plane with no $\hat{\mathbf{Z}}$ motion, or the lobe is improperly defined. We can expect only ratios between 0 and 1 and $\tilde{T}_{\max}$ between 0 and 0.5 of the chief orbit. This will be used as a constraint on the $\hat{\mathbf{Z}}$ motion.

C. Entry and Exit Conditions

A variety of entry and exit conditions into and out of the lobe can be formulated. The method by which the entry and exit relative positions and velocities are defined will have an effect on the cost function. For brevity, only three general categories are explored here: 1) the defined entry/exit condition, 2) the open entry/exit condition, and 3) the repeating hover orbit.

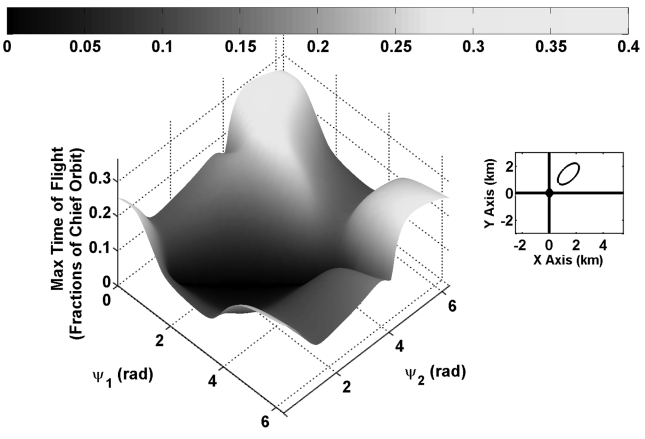

Fig. 3 Surface of maximum time of flight between ψ_1 and ψ_2 ($\alpha = 45$ deg, $\gamma = 2$ km, $\tau_x = 1$ km, and $\tau_y = 0.5$ km).

The first condition enables the user to specify the relative position and velocity of the deputy at either the entry or exit of the lobe (or both). Thus, in addition to the lobe parameters the user must also specify

$$\psi_1,\ (\dot{\tilde{x}}_1^-, \dot{\tilde{y}}_1^-) \quad \text{and/or} \quad \psi_k,\ (\dot{\tilde{x}}_{k+1}^+, \dot{\tilde{y}}_{k+1}^+) \tag{28}$$

In general, the user can specify any relative velocity; however, the results presented here assume entry to and/or exit from a closed-relative orbit centered on the chief satellite. This is done by setting the secular and constant terms in Eq. (9b) to zero and solving for the necessary initial velocities. The result is

$$\dot{\tilde{x}}_o = \pi\tilde{y}_o \qquad \dot{\tilde{y}}_o = -4\pi\tilde{x}_o \tag{29}$$

Note that this also zeros out the constant term in Eq. (9a). There are two benefits to calculating the entry/exit relative velocities in this manner. First, it provides reasonable relative velocities with which to work and, second, the velocities and subsequent solution are independent of the orbital radius. The open condition puts no restrictions at all on the starting relative position and velocity; thus, the algorithm is free to choose these in whatever manner is most optimal. The repeating hover orbit constrains the solution such that the final relative position and velocity are the same as the entry conditions; thus, the deputy can stay in a repeatable trajectory for as long as the user requires.

D. Continuous-Thrust Benchmark

To assess the value of an optimized discrete-thrust solution, a benchmark is established. The benchmark is based on a continuous-thrust solution whereby the deputy maintains a stationary position at a desired coordinate. The continuous-thrust solution is linear in x and z; thus, the smallest values allowed by the lobe are used. Applying the scaling in Eq. (20) to Eq. (15) to find the specific ΔV yields

$$\Delta\check{V}_C = (1/2\pi)(12\tilde{x}_{\min} + 4\tilde{z}_{\min})\pi^2\tilde{T}_T = (6\tilde{x}_{\min} + 2\tilde{z}_{\min})\pi\tilde{T}_T \tag{30}$$

This equation works well if we assume that the deputy starts at the minimum x and z values; however, to use this as a fair comparison, we must include the ΔV needed to get into that position. Assume that the continuous-thrust solution starts at the same entry position and velocity as the discrete-thrust solution. The ΔV required to get to $\tilde{x}_{\min}$ is found using the pre- (−) and post- (+) relative velocities:

$$\begin{aligned}\Delta\check{V}_1^2 &= \frac{1}{4\pi^2}[(\dot{\tilde{x}}_1^+ - \dot{\tilde{x}}_1^-)^2 + (\dot{\tilde{y}}_1^+ - \dot{\tilde{y}}_1^-)^2] \\ &= \frac{1}{4\pi^2}[\dot{\tilde{x}}_1^+ - \dot{\tilde{x}}_1^- \quad \dot{\tilde{y}}_1^+ - \dot{\tilde{y}}_1^-]\begin{bmatrix}\dot{\tilde{x}}_1^+ - \dot{\tilde{x}}_1^- \\ \dot{\tilde{y}}_1^+ - \dot{\tilde{y}}_1^-\end{bmatrix}\end{aligned} \tag{31}$$

where [see Eq. (10)]

$$\begin{bmatrix}\dot{\tilde{x}}_1^+ - \dot{\tilde{x}}_1^- \\ \dot{\tilde{y}}_1^+ - \dot{\tilde{y}}_1^-\end{bmatrix} = \begin{bmatrix}\frac{-4\tilde{S}+6\pi\tilde{T}\tilde{C}}{8-6\pi\tilde{T}\tilde{S}-8\tilde{C}} & \frac{4\tilde{S}-6\pi\tilde{T}}{8-6\pi\tilde{T}\tilde{S}-8\tilde{C}} & \frac{-2+2\tilde{C}}{8-6\pi\tilde{T}\tilde{S}-8\tilde{C}} \\ \frac{-14+12\pi\tilde{T}\tilde{S}+14\tilde{C}}{8-6\pi\tilde{T}\tilde{S}-8\tilde{C}} & \frac{2-2\tilde{C}}{8-6\pi\tilde{T}\tilde{S}-8\tilde{C}} & \frac{\tilde{S}}{8-6\pi\tilde{T}\tilde{S}-8\tilde{C}}\end{bmatrix} \times \begin{bmatrix}\tilde{x}_1 \\ \tilde{x}_2 \\ \Delta\tilde{y}\end{bmatrix} - \begin{bmatrix}\dot{\tilde{x}}_1^- \\ \dot{\tilde{y}}_1^-\end{bmatrix} \tag{32}$$

and $\Delta\tilde{y} = \tilde{y}_2 - \tilde{y}_1$, $\tilde{S} = \sin(2\pi\tilde{T}_{1,2})$, and $\tilde{C} = \cos(2\pi\tilde{T}_{1,2})$. The time of flight is found by using the FMINCON function in MATLAB® to minimize $\Delta\check{V}_1$ while applying the constraint developed in Sec. II.C. Once at $\tilde{x}_{\min}$, the deputy must make a burn to cancel its relative velocity, which is equal in magnitude but opposite in direction to the final velocity of the previous leg:

$$\Delta\breve{V}_2^2 = (1/4\pi^2)\|\dot{\tilde{x}}_2^-\hat{\mathbf{X}} + \dot{\tilde{y}}_2^-\hat{\mathbf{Y}}\|_2^2 \tag{33}$$

where

$$\begin{bmatrix}\dot{\tilde{x}}_2^- \\ \dot{\tilde{y}}_2^-\end{bmatrix} = \begin{bmatrix}\frac{-4\tilde{S}+6\pi\tilde{T}}{8-6\pi\tilde{T}\tilde{S}-8\tilde{C}} & \frac{4\tilde{S}-6\pi\tilde{T}\tilde{C}}{8-6\pi\tilde{T}\tilde{S}-8\tilde{C}} & \frac{2-2\tilde{C}}{8-6\pi\tilde{T}\tilde{S}-8\tilde{C}} \\ \frac{2-2\tilde{C}}{8-6\pi\tilde{T}\tilde{S}-8\tilde{C}} & \frac{-14+12\pi\tilde{T}\tilde{S}+14\tilde{C}}{8-6\pi\tilde{T}\tilde{S}-8\tilde{C}} & \frac{\tilde{S}}{8-6\pi\tilde{T}\tilde{S}-8\tilde{C}}\end{bmatrix}\begin{bmatrix}\tilde{x}_1 \\ \tilde{x}_2 \\ \Delta\tilde{y}\end{bmatrix} \tag{34}$$

The exit leg will either be the natural drift out of the lobe for the open exit condition (requiring no ΔV) or an impulsive thrust to get to a defined exit position and leave the lobe with the required exit velocity. These are calculated similar to the entry burns. The remainder of the time is spent hovering at $(\tilde{x}_{\min}, \tilde{z}_{\min})$; thus,

$$\Delta\breve{V}_C = 6x_{\min}\pi(\tilde{T}_T - \tilde{T}_{\text{entry}} - \tilde{T}_{\text{exit}}) \tag{35}$$

This allows the benchmark solution to have the same total time of flight as the discrete solution. The total ΔV from these three parts is then used as the comparison.

E. Optimization Method

The proposed optimization method first solves the problem in the $\hat{\mathbf{X}}\,\hat{\mathbf{Y}}$ plane. The user chooses the lobe parameters, entry/exit conditions (with the additional parameters as appropriate), and total number of proposed legs (k). The cost function is minimized using the FMINCON function in MATLAB® with the maximum time of flight constraint developed in Sec. II.C to bound $\tilde{T}$ for each leg. $\Delta\breve{V}$ is calculated using only the linear CW dynamics with no perturbations. The output is a set of thrust locations (ψ) and the times of flight between them. These elements completely define the trajectories.

Recall that motion in the $\hat{\mathbf{Z}}$ direction is a harmonic oscillator that affords a single degree of freedom with which to optimize the problem. The period of the $\hat{\mathbf{Z}}$ oscillation ($\tilde{P}_z$) is chosen as the optimization parameter based on the following argument. Assume the $\hat{\mathbf{X}}\,\hat{\mathbf{Y}}$ plane optimization has yielded a total time of flight ($\tilde{T}_T$). We desire the deputy to stay between $\tilde{z}_{\min}$ and $\tilde{z}_{\max}$ for the same amount of time. The minimum number of burns required is

$$\text{no. of burns} = \lfloor \tilde{T}_T/\tilde{P}_z \rfloor \tag{36}$$

It can be shown that the minimum ΔV required for each of these burns is

$$\Delta\breve{V}_i = 2\tilde{z}_{\min}\tan(\pi\tilde{P}_z) \tag{37}$$

A derivation is provided in the Appendix [see Eq. (A10)]. Assuming no entry burn is required, the total number of burns required will be $k_z - 1$, where k_z is the number of oscillations in the $\hat{\mathbf{Z}}$ direction. The total ΔV is

$$\Delta\breve{V}_Z = 2\tilde{z}_{\min}(k_z - 1)\tan(\pi\tilde{P}_z) = 2\tilde{z}_{\min}(k_z - 1)\tan(\pi\tilde{T}_T/k_z) \tag{38}$$

Noting that $\tilde{P}_z$ is a multiple of the total time of flight, we can write the following relationship:

$$(1/\tilde{k}_z)T_T = \tilde{P}_z \tag{39}$$

$\Delta\breve{V}_Z$ is inversely proportional to $\tilde{P}_z$; thus, we desire the largest possible period (or fewest number of bounces, k_z) without exceeding the maximum period defined by Eq. (27). An example problem is found in Fig. 4. Assume that the $\hat{\mathbf{X}}\,\hat{\mathbf{Y}}$ optimization has yielded a total time of flight of $\tilde{T}_T = 0.45$, $\tilde{z}_{\min} = 1$, and $\tilde{z}_{\max} = 1.25$. Thus, the $\hat{\mathbf{Z}}$ motion is constrained to have the following relationship:

$$\tilde{P}_z < \tilde{T}_{\max} = \frac{1}{\pi}\cos^{-1}(0.8) \approx 0.2 \tag{40}$$

Reading from Fig. 4, the smallest possible total $\Delta\breve{V}_Z$ that stays under the constraint occurs at

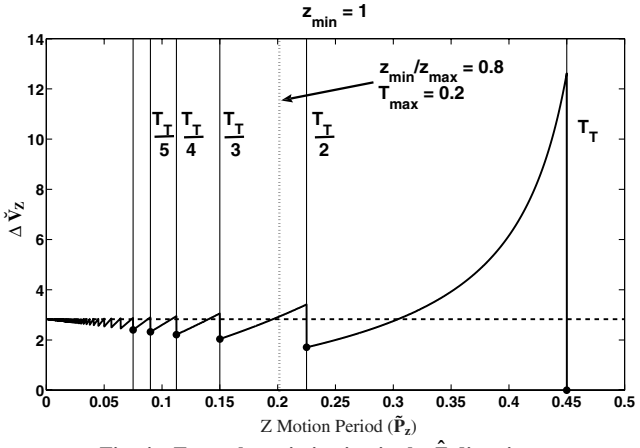

Fig. 4 Example optimization in the $\hat{\mathbf{Z}}$ direction.

$$\tilde{P}_z = \tilde{T}_T/3 = 0.15 \tag{41}$$

The horizontal line is the $\Delta\breve{V}$ required for a continuous-thrust hover at $\tilde{z}_{\min}$ and is equal to

$$\Delta\breve{V}_C = 2\tilde{z}_{\min}\pi\tilde{T}_T \tag{42}$$

Note how the discrete solution converges to the continuous-thrust line as $\tilde{P}_z \to 0$, that is, as the number of legs (k_z) goes to infinity.

III. Results

With an understanding of the dynamics and solution method in hand, we turn next to analyzing the results and drawing conclusions. Recall that, due to the form of the equations of motion, these results are applicable to a circular chief orbit of any size and about any celestial body assuming that inverse-squared gravity is the only force of significance. First, results are presented for the special class of hovering orbits that take advantage of the equilibrium conditions of the equations of motion (lobe 1). Next, the optimal trajectories for defined/open and open/repeat cases as applied to lobes 2 and 3 are given. See Table 1 and Fig. 5 for the lobe parameters.

A. Persistent Hover Orbit

If the lobe happens to intersect the $\hat{\mathbf{Y}}$ axis, then the optimal solution (for the linear CW case) is to stay on that $\hat{\mathbf{Y}}$ axis, which is, in fact, the loci of equilibrium points.

Lobes that contain some portion of the $\hat{\mathbf{Y}}$ axis deserve special consideration. First, let us examine the output of the optimization algorithm when given a lobe that intersects the $\hat{\mathbf{Y}}$ axis. Figure 6 is the result of an optimization run for a defined entry ($\psi_1 = \pi/4$) and open exit on lobe 1. Assume the deputy is already on a near relative orbit that intersects the user-defined lobe. For this example, the entry relative velocity is arbitrarily chosen such that the deputy enters from a closed-relative orbit centered on the chief at ψ_1. There is nothing special about this choice of entry conditions; it is simply convenient for calculation. The result is, not surprisingly, to place the deputy on the natural 2×1 ellipse predicted by the Clohessy–Wiltshire equations of motion when the deputy and chief periods are matched [8]. This special case relative orbit is called a persistent hover orbit (PHO), defined as any natural closed orbit that fits entirely within the lobe. The PHO is a type of repeating hover orbit that does not require any impulsive thrusting to maintain, other than what is required to

Table 1 Lobe parameters

Lobe no.	α, deg	β, deg	γ, km	τ_x, km	τ_y, km	η, deg
1	90	90	2	1	0.5	20
2	45	90	2	1	0.5	45
3	45	90	2	0.5	1	45

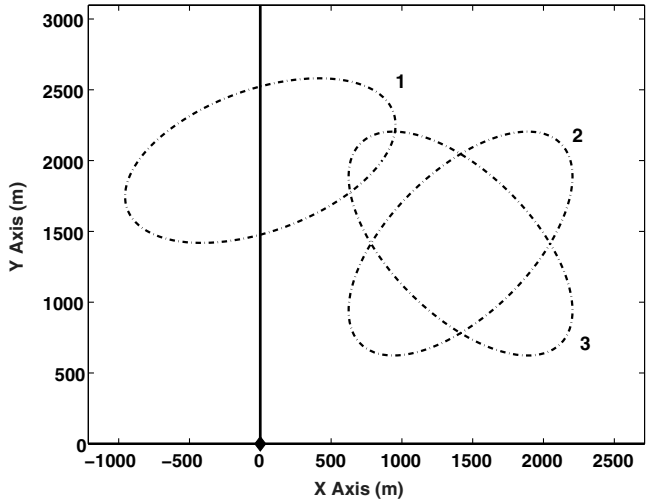

Fig. 5 Lobes used in the results.

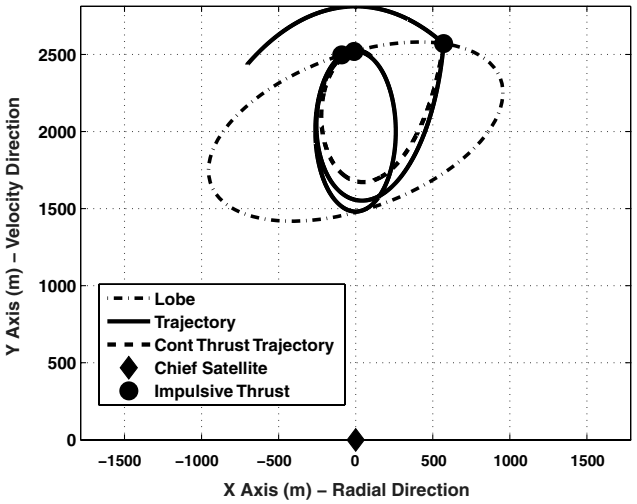

Fig. 6 PHO optimization results for lobe 1.

correct for perturbations and linearization errors, making it ideal for long-term proximity operations. The PHO is specified by two parameters as shown in Fig. 7: the semiminor axis (ρ) and the center coordinate along the $\hat{\mathbf{Y}}$ axis (b). In the limit as $\rho \to 0$, the PHO becomes a point on the $\hat{\mathbf{Y}}$ axis. The PHO optimization problem is as follows. Assume the deputy's trajectory intersects the lobe at a defined entry position and relative velocity. Positioning the deputy onto the PHO requires two impulsive thrusts, the first at lobe entry to place the deputy on a trajectory toward the PHO and another to enter it. For a given PHO with a known entry position and velocity, only two parameters are required to define these burns: 1) time of flight from lobe entry to PHO entry and 2) PHO entry point. Using these parameters in Eqs. (10) and (11), we have all the information needed to calculate the specific ΔV. This greatly simplifies our optimization routine because we can globally search for the minimum-fuel solution of these two burns. The only remaining question is, what are the best values of the PHO semiminor axis (ρ) and center position (b).

Results indicate that the minimum-fuel answer is to choose ρ and b such that ρ is as large as possible. Figures 8 and 9 present the results of evaluating all values of ρ and b that yield PHOs that are completely contained inside lobe 1. Figures 8a and 9a are the $\Delta\check{V}$ surface over ρ and b, whereas Figs. 8b and 9b show the resultant minimum-fuel trajectory. Note that only combinations of ρ and b that fit completely inside the lobe are evaluated, and the stair step feature is due to the discretization of the search space. In both cases, the minimum $\Delta\check{V}$ occurred when the largest possible ρ value was

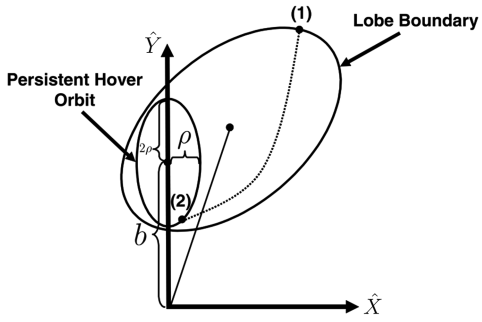

Fig. 7 Persistent hover orbit.

chosen. Note that this implies a value of b such that the center of the PHO in the $\hat{\mathbf{Y}}$ direction will be halfway between the two points at which the lobe intersects the $\hat{\mathbf{Y}}$ axis. The results for several different cases with defined conditions show that, if mission requirements dictate a fairly small time of flight, then optimizing the cost function over one or two legs may still yield the lowest total fuel solution; however, if a longer total time of flight is required, searching for the minimum two-thrust solution to place the deputy onto a PHO is optimal regardless of entry/exit conditions. The next two sections, which combine the entry/exit conditions developed in Sec. II.C, present results for the following two cases: 1) defined open and 2) open repeat.

B. Case 1: Defined Entry/Open Exit

Case 1 investigates trajectories for which the entry condition is defined, the exit condition is left open, and the lobe does not intersect the $\hat{\mathbf{Y}}$ axis. Recall that the defined entry condition requires the user to provide an incoming relative velocity at a specified lobe entry point. For convenience and because the choice of this initial condition is arbitrary, the following results will use the relative velocity of the closed-relative orbit that intersects the lobe at the specified point and is centered on the chief. Case 1 is of particular interest because, for the single leg case, there are only two optimization parameters (ψ_2 and $\tilde{T}_{1,2}$); thus, we can visualize the cost surface (Fig. 10a) and watch the iteration path (the dashed line) of the nonlinear programming algorithm toward the optimal solution (indicated by a diamond).

The results of the optimization algorithm for lobes 2 and 3 under the conditions already specified are shown in Figs. 10a and 11a; the solid line on the cost contour plot indicates the maximum time of flight for each value of ψ_2, and the lobe entry point is defined as $\psi_1 = \pi/4$. This curve is the slice, at $\psi_1 = \pi/4$, of a constraint surface similar to Fig. 3. Note that in both cases there is a local minimum with a very short time of flight between 5 and 6 rad. This represents the trivial solution of the deputy passing through the lobe with no thrust at the entry point, resulting in a cost function of $J = 0$.

The next set of graphs (Figs. 12–17) show the evolution of the trajectories for lobes 2 and 3 as the number of legs is increased. The left-hand plots show the lowest cost discrete trajectory found after searching through multiple initial condition choices. The right-hand plots show the cumulative specific ΔV incurred over time for the discrete and continuous-thrust trajectories. The continuous-thrust solution is described in Eq. (35) and is a function only of the lobe shape, position, orientation, and entry position and velocity. In general, it consists of an entry leg to the $\tilde{x}_{\min}$ coordinate, possible hovering at $\tilde{x}_{\min}$, and then exiting the lobe either at a designated point, drifting out of the lobe, exiting onto another closed-relative orbit, or remaining at $\tilde{x}_{\min}$. These thrusts are based on minimum ΔV solutions. The continuous solution entry and exit legs will both have a fixed time of flight (again based on the minimum ΔV solution). The difference between the sum of these two legs and the total time of flight of the discrete-thrust solution is made up by hovering with continuous thrust at $\tilde{x}_{\min}$. Because there is no minimum total time of flight constraint applied to the cost function, it is possible that the sum of the entry and exit legs is greater than the time of flight found in the optimization routine. In this case, no hovering is required and the

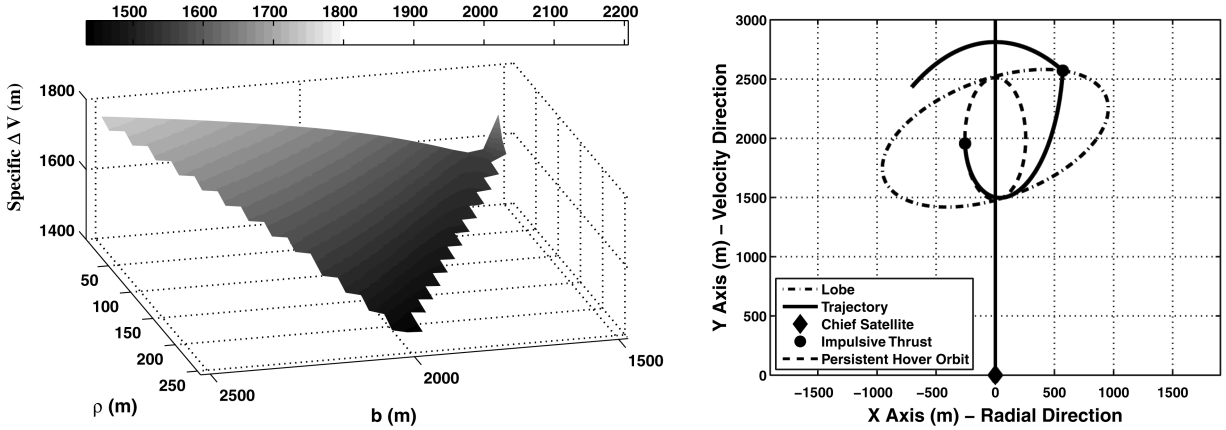

a) $\Delta\check{V}$ as a function of ρ and b

b) The minimum $\Delta\check{V}$ trajectory

Fig. 8 Optimal PHO results for lobe 1 ($\psi_1 = \pi/4$).

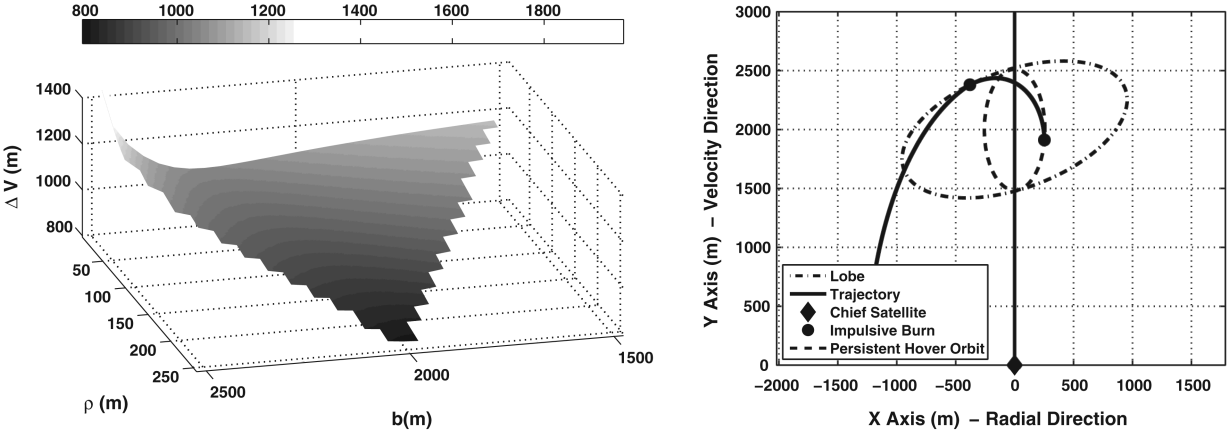

a) $\Delta\check{V}$ as a function of ρ and b

b) The minimum $\Delta\check{V}$ trajectory

Fig. 9 Optimal PHO results for lobe 1 ($\psi_1 = 3\pi/4$).

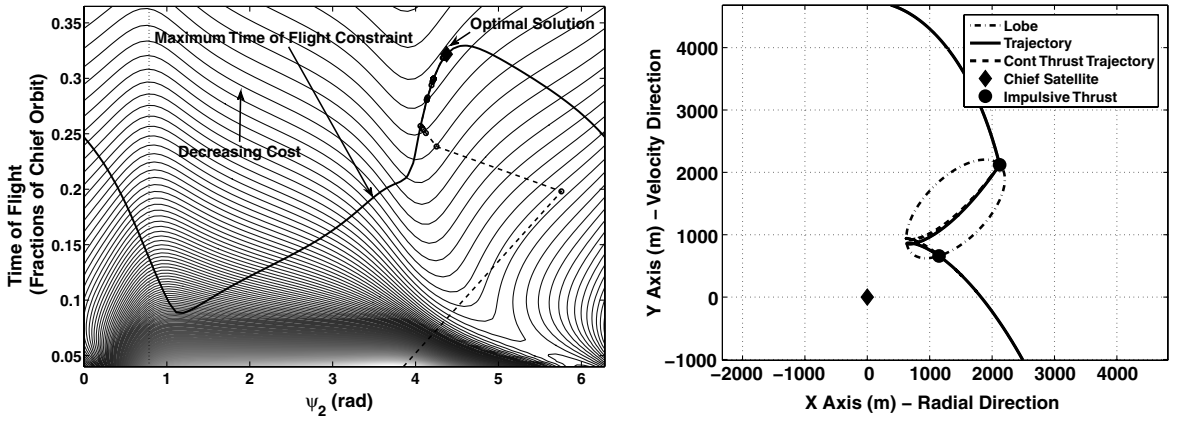

a) Cost function and optimization iterations

b) Optimal discrete trajectory

Fig. 10 Results for defined entry/open exit (case 1): lobe 2, single leg.

continuous-thrust time of flight will be longer than the discrete solution. Care must be taken when comparing the discrete and continuous solutions in these cases.

Figures 12–14 show the evolution of the trajectories for lobe 2 as the number of legs increases from one to five. There are minor changes in the trajectory and performance as more legs are requested, but there is a definite pattern of convergence toward a final trajectory. In all but the single leg case, the continuous solution outperforms the discrete case. Also, all but the five-leg simulation runs into the problem discussed earlier with the time of flight of the entry and exit legs of the continuous solution being larger than the entire discrete time of flight. It is clear that, for lobe 1, a continuous-thrust strategy is more efficient for all but the single-leg case.

Figures 15–17 are trajectories within lobe 3. Again, there is clear convergence to a final trajectory but, unlike in the previous case, there are slight fuel savings by using the discrete solution in all but

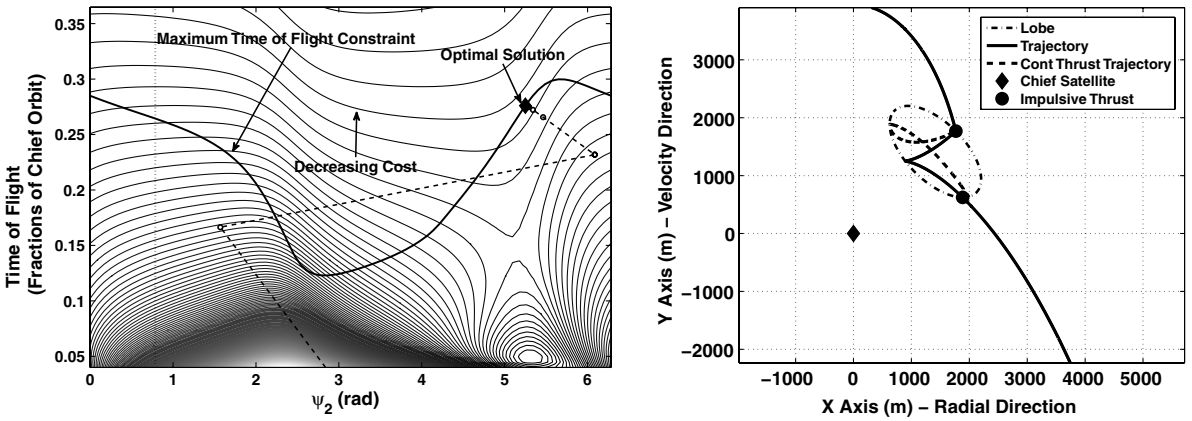

a) Cost function and optimization iterations b) Optimal discrete trajectory

Fig. 11 Results for defined entry/open exit (case 1): lobe 3, single leg.

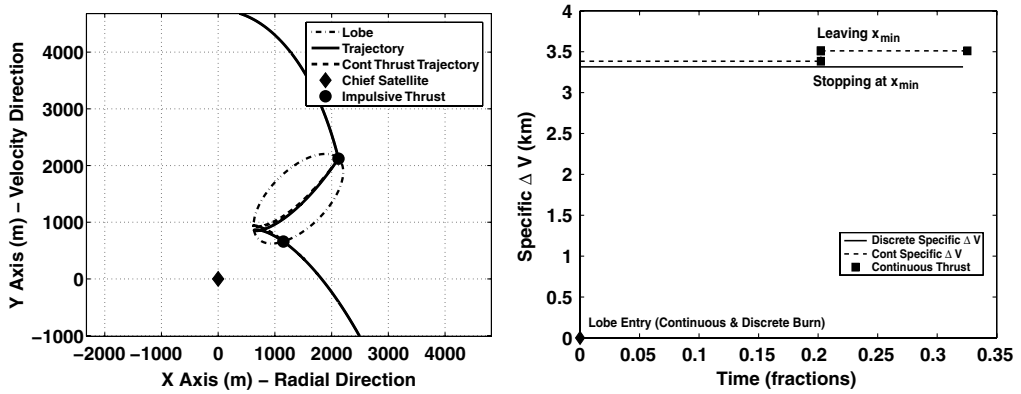

a) $\hat{X}\hat{Y}$ plane trajectory b) Growth of $\Delta\check{V}$

Fig. 12 Results for defined entry/open exit (case 1): lobe 2, single leg.

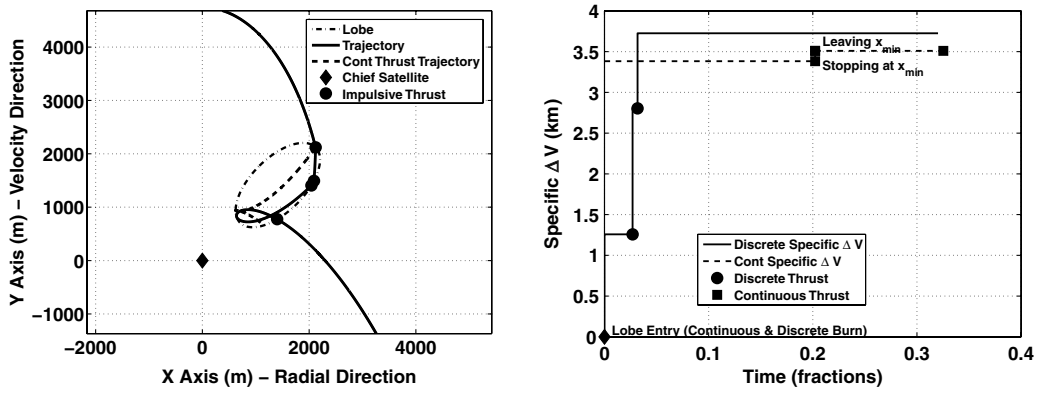

a) $\hat{X}\hat{Y}$ plane trajectory b) Growth of $\Delta\check{V}$

Fig. 13 Results for defined entry/open exit (case 1): lobe 2, legs = 3.

the final ($k = 5$) simulation. This set of runs is also a good example of how additional legs are accommodated by clustering several smaller thrusts to take the place of one larger thrust. In most cases, this is significantly less efficient, a fact notably displayed in Fig. 17. In the one- and three-leg trajectories, the first leg from the entry point to near the top of the lobe is the result of a single thrust. When $k = 5$, this single thrust is split into three thrusts. Although the time of flight and trajectory of this leg remain nearly identical, the fuel spent is nearly 70% greater in the latter case. This splitting phenomenon is due to the unrestricted bounds on each leg's time of flight and $\Delta\check{V}$. With no minimum time of flight, optimal trajectories are split into smaller pieces to satisfy the requirement for more legs. This is a shortcoming of the cost function as posed and should be addressed in future work. The splitting effect makes it clear that, although there are some increases to time of flight, there is a distinct k after which there is no improvement.

C. Case 2: Open Entry/Repeating Hover

By specifying open entry/repeating hover, we seek to find closed trajectories that can be sustained for as long as the mission planner desires and the deputy's fuel stores last. This is done by constraining the relative position and velocity at the final point (postthrust) to be the same as the initial relative position and velocity. These closed

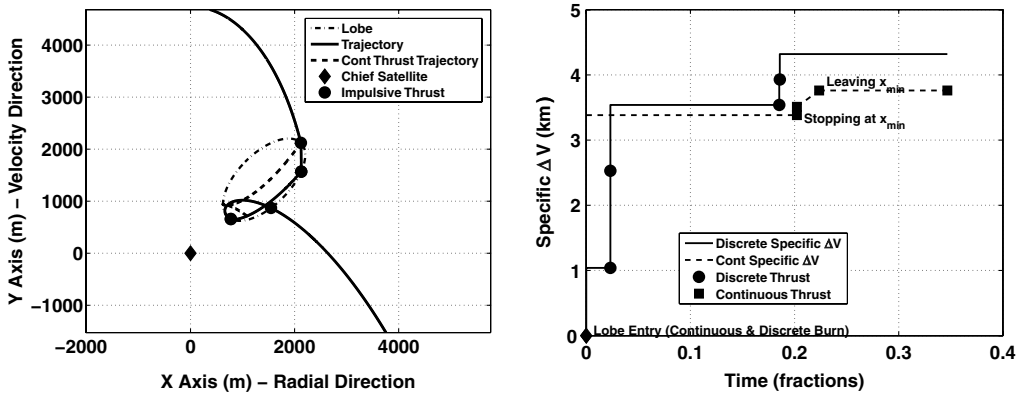

a) $\hat{X}\hat{Y}$ plane trajectory b) Growth of $\Delta\check{V}$

Fig. 14 Results for defined entry/open exit (case 1): lobe 2, legs = 5.

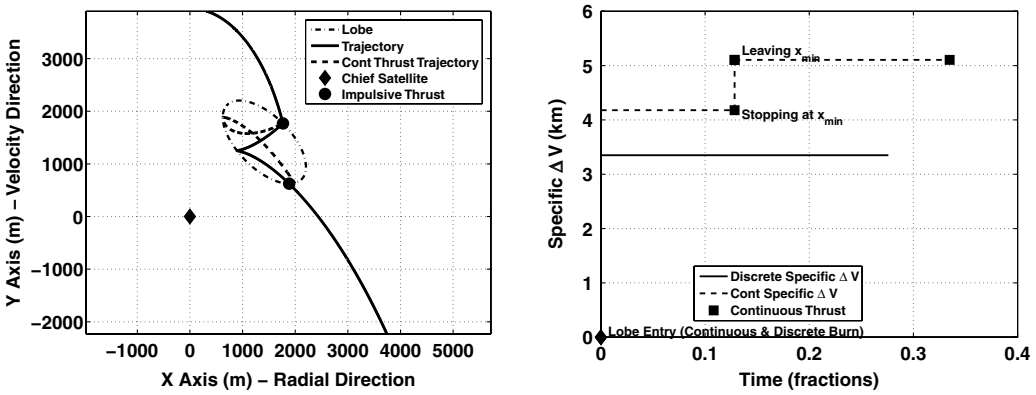

a) $\hat{X}\hat{Y}$ plane trajectory b) Growth of $\Delta\check{V}$

Fig. 15 Results for defined entry/open exit (case 1): lobe 3, single leg.

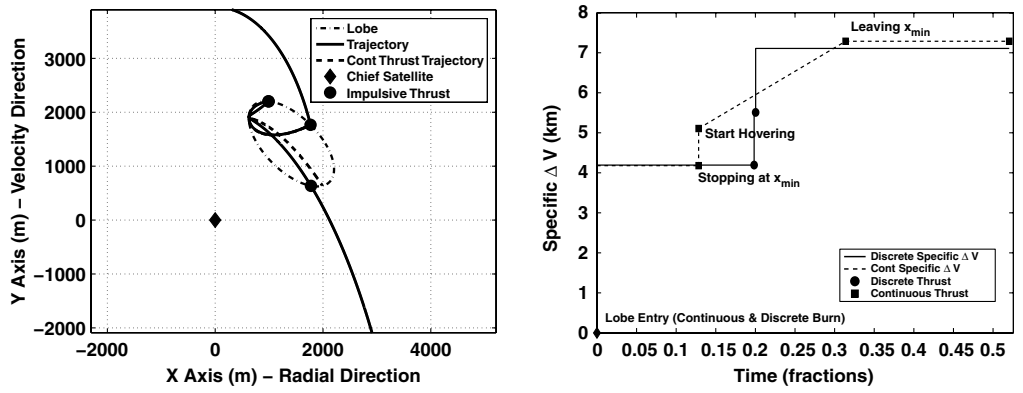

a) $\hat{X}\hat{Y}$ plane trajectory b) Growth of $\Delta\check{V}$

Fig. 16 Results for defined entry/open exit (case 1): lobe 3, legs = 3.

trajectories are recommended when simply increasing the number of legs does not yield the needed total time of flight. The optimization algorithm yields two types of closed-relative orbits. The first is the classic teardrop, in which the trajectory intersects itself at a single point (Fig. 18) [3,4], providing an opportunity to perform an impulsive thrust and repeat the teardrop. The second is the bounce trajectory (Fig. 19), in which the deputy bounces back and forth between two points. The teardrop trajectory outperforms the bounce and is the focus of further discussion.

Just as the PHO tends to be the most efficient trajectory for a lobe encompassing an equilibrium condition, the teardrop trajectory tends to be the lowest cost solution for a repeating hover condition. Note that in Figs. 18–20 the teardrop paths are not perfect (i.e., commensurate with CW dynamics), but reflect numerical imprecisions inherent in a nonlinear programming solution. This encourages analysis of all possible teardrops and their cycle cost (ΔV per cycle). Figure 21 presents the results of that analysis. In each example, only ψ that have $\tilde{T}_{\max}(\psi_1, \psi_1) > 0$ are evaluated and only for $\tilde{T} < \tilde{T}_{\max}(\psi_1, \psi_1)$, thus producing regions of no data in the cost surface. That cost surface, as seen in Fig. 21a, shows that, although there is a single global minimum, a family of nearly identical cost teardrops are available to a mission planner. Thus, if cycle period is an important mission parameter, a wide range of values can be selected with only small changes to cycle cost. Figure 21b displays a

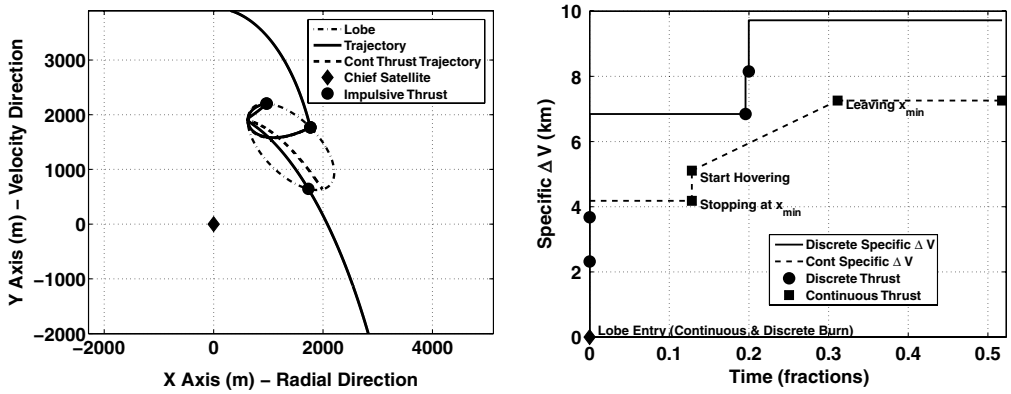

a) $\hat{\mathbf{X}}\hat{\mathbf{Y}}$ plane trajectory b) Growth of $\Delta\check{V}$

Fig. 17 Results for defined entry/open exit (case 1): lobe 3, legs = 5.

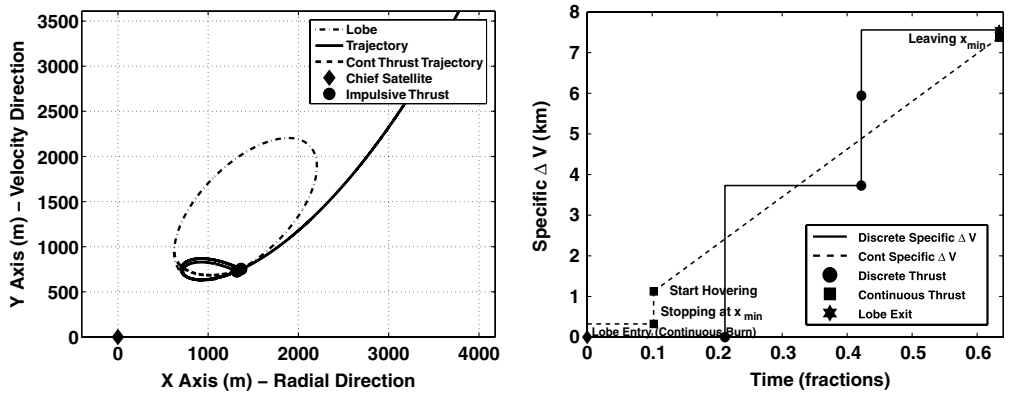

a) $\hat{\mathbf{X}}\hat{\mathbf{Y}}$ plane trajectory b) Growth of $\Delta\check{V}$

Fig. 18 Results for open entry/repeating (case 2): lobe 2, legs = 3, teardrop.

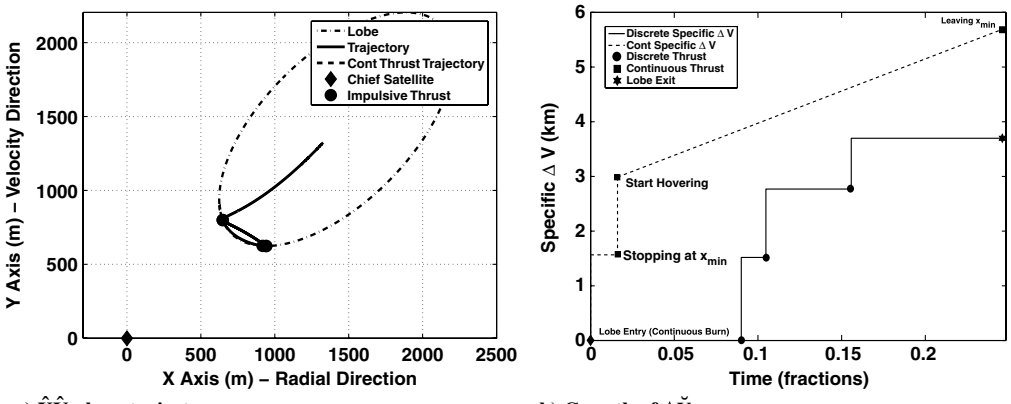

a) $\hat{\mathbf{X}}\hat{\mathbf{Y}}$ plane trajectory b) Growth of $\Delta\check{V}$

Fig. 19 Results for open entry/repeating (case 2): lobe 2, legs = 2, bounce.

representative of this family of choices chosen for its larger time of flight. Figure 21c demonstrates the repeating pattern of the relative specific velocities.

It has been shown that thrusting repeatedly at the apex of the teardrop to remain on that relative orbit incurs the same cumulative ΔV as thrusting continuously at the time-averaged x coordinate (centroid) of the teardrop [4]:

$$\bar{x}_{\mathrm{TD}} = \frac{1}{\tilde{T}_{\mathrm{TD}}}\int_0^{\tilde{T}_{\mathrm{TD}}} \tilde{x}(\tilde{t})\,\mathrm{d}\tilde{t} = \frac{2(1-\tilde{C})\tilde{x}_o}{8 - 6\pi\tilde{T}_{\mathrm{TD}}\tilde{S} - 8\tilde{C}} \tag{43}$$

This $\bar{x}_{\mathrm{TD}}$ will always be farther from the $\hat{\mathbf{Y}}$ axis than $x_{\min}$; therefore, in the long run, thrusting continuously at $x_{\min}$ will require less fuel. Ultimately, the choice of thrust locations will rest on the teardrop entry/exit conditions. It is, in general, more fuel intensive to stop at $x_{\min}$ than to divert the trajectory onto a teardrop. The total $\Delta\check{V}$ per cycle can be found in closed form [see Eq. (23)]:

$$\Delta\check{V}_{\mathrm{TD}} = 6\pi\tilde{T}_{\mathrm{TD}}\bar{x}_{\mathrm{TD}} = \frac{12\pi\tilde{T}_{\mathrm{TD}}(1-\tilde{C})\tilde{x}_o}{8 - 6\pi\tilde{T}_{\mathrm{TD}}\tilde{S} - 8\tilde{C}} \tag{44}$$

This cumulative $\Delta\check{V}$ is plotted in Fig. 21d and tracks exactly with the stair step of the discrete-thrust solution. Also plotted is the cumulative $\Delta\check{V}$ for the continuous solution at $x_{\min}$. Figure 21d can be used to evaluate whether to use the discrete or continuous solution in an actual mission scenario. Note that these solutions assume that the deputy started in the desired position (at the start of the teardrop for

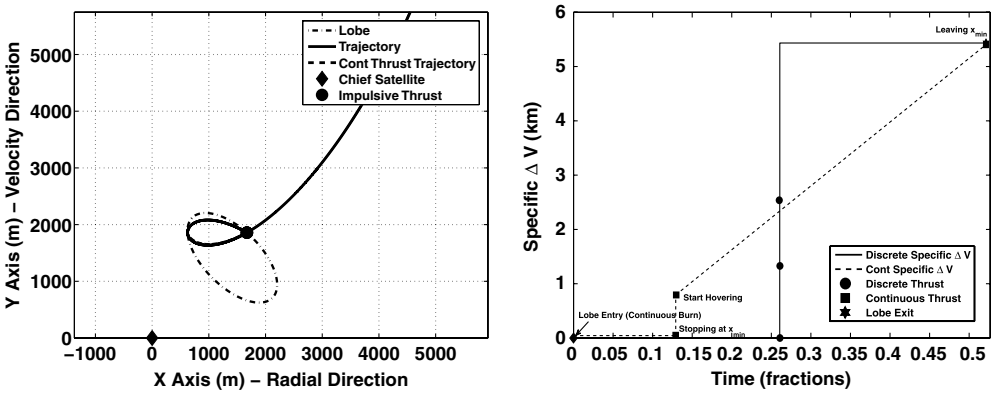

a) $\hat{X}\hat{Y}$ plane trajectory b) Growth of $\Delta\breve{V}$

Fig. 20 Results for open entry/repeating (case 2): lobe 3, legs = 3, teardrop.

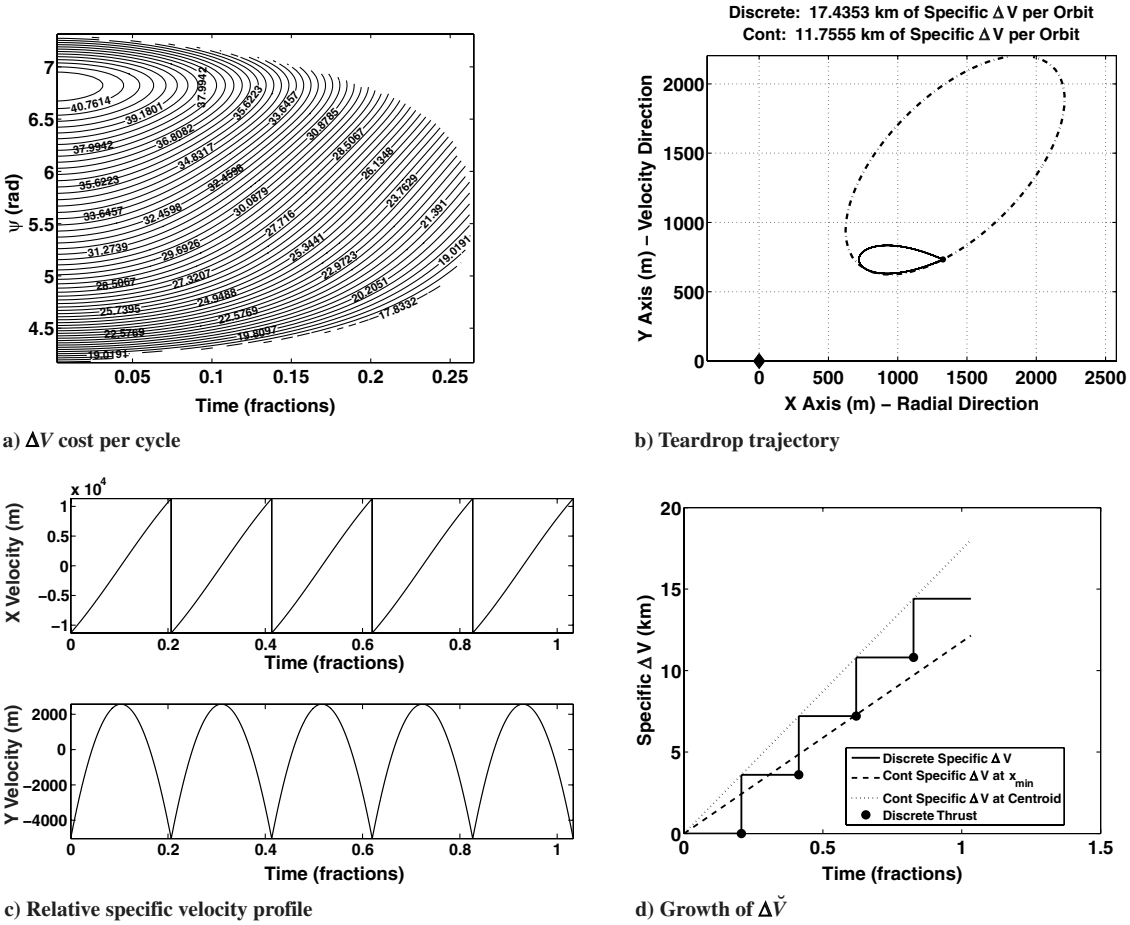

a) ΔV cost per cycle b) Teardrop trajectory

c) Relative specific velocity profile d) Growth of $\Delta\breve{V}$

Fig. 21 Teardrop analysis for lobe 2.

discrete and at $\tilde{x}_{\min}$ for the continuous) with the desired relative velocity. Fuel usage to get to those initial conditions, however, must be taken into account. That minimum-fuel solution is treated here as a simple constant added to a linear function that will shift the $\Delta\breve{V}$ growth profiles up. They will not, in general, be the same for the continuous and discrete solutions. The total fuel used in the discrete solution will be

$$\Delta\breve{V}_{\text{Discrete}} = \Delta\breve{V}_D\lfloor\tilde{T}_T/P_D\rfloor + \Delta\breve{V}_{D_{IC}} \tag{45}$$

where $\Delta\breve{V}_D$ is the specific ΔV required at each teardrop burn, $\tilde{T}_T$ is the total time of flight required, P_D is the period of the teardrop, and $\Delta\breve{V}_{D_{IC}}$ is the ΔV required to get into position for the first teardrop.

The continuous solution is

$$\Delta\breve{V}_C = 6\tilde{x}_{\min}\pi\tilde{T}_T + \Delta\breve{V}_{C_{IC}} \tag{46}$$

where $\Delta\breve{V}_{C_{IC}}$ is the ΔV required to get to and stop at $x_{\min}$. For the discrete-thrust solution to be the fuel-optimal choice, we need

$$\Delta\breve{V}_{\text{Discrete}} < \Delta\breve{V}_C \tag{47}$$

$$\lfloor\tilde{T}_T/P_D\rfloor < \frac{6\tilde{x}_{\min}\pi\tilde{T}_T + \Delta\breve{V}_{C_{IC}} - \Delta\breve{V}_{D_{IC}}}{\Delta\breve{V}_D} \tag{48}$$

This, then, is the criterion for choosing between a discrete and

continuous solution. As total time of flight increases, the continuous solution will eventually outperform the discrete, but, for a shorter total time of flight, it may be more efficient to use a discrete strategy.

IV. Conclusions

Proximity operations and hovering specifically are fuel-expensive operations to perform and will only be undertaken when mission needs are great. This work investigates a method to keep fuel costs as low as possible when hovering within a desired lobe in relative space. The results have shown that practical hovering orbits produced with impulsive thrusts require a ΔV comparable with a continuous-thrust benchmark. The choice of discrete versus continuous strategy is highly dependent on lobe entry and exit conditions, and decisions are easily made by comparing the cumulative ΔV for both strategies. Note also that, because ΔV is linear in the $\hat{\mathbf{X}}$ and $\hat{\mathbf{Z}}$ coordinates, the farther away the lobe is placed from the chief, the more expensive the hovering maneuver. Hardware and mission requirements will also factor heavily into this decision. For the analyst, the continuous-thrust solution provides an excellent estimate of the ΔV required to hover inside a specified lobe. This solution is robustly and rapidly calculated without any precomputing of the constraint surface. That estimate can be scaled by the inverse of the chief's mean motion to get the actual ΔV cost for an orbit with a given size. The ability to compare all possible sizes of chief orbits greatly extends the applicability of this research.

Appendix: Derivation of $\tilde{T}_{\max}$ and ΔV for $\hat{\mathbf{Z}}$ Motion

The $\hat{\mathbf{Z}}$ motion is decoupled from the $\hat{\mathbf{X}}$ $\hat{\mathbf{Y}}$ motion and can be treated separately. The closed-form solution of the position is Eq. (9):

$$\tilde{z}(\tilde{t}) = \frac{\dot{\tilde{z}}_o}{2\pi}\sin(2\pi\tilde{t}) + \tilde{z}_o\cos(2\pi\tilde{t}) = \sqrt{\left(\frac{\dot{\tilde{z}}_o}{2\pi}\right)^2 + \tilde{z}_o^2}\cos\left[2\pi\tilde{t} - \tan^{-1}\left(\frac{\dot{\tilde{z}}_o}{2\pi z_o}\right)\right] \tag{A1}$$

Pulling the amplitude information from this equation and setting it equal to $\tilde{z}_{\max}$,

$$\tilde{z}_{\max} = \sqrt{\left(\frac{\dot{\tilde{z}}_o}{2\pi}\right)^2 + \tilde{z}_o^2} \tag{A2}$$

Rearranging

$$\sqrt{\left(\frac{\tilde{z}_{\max}}{\tilde{z}_o}\right)^2 - 1} = \frac{\dot{\tilde{z}}_o}{2\pi\tilde{z}_o} \tag{A3}$$

which is a term we will use shortly. Assume a cylinder is defined as shown in Fig. 1b, in which h is half the height of the cylinder ($h > 0$) and β is the angle between the $\hat{\mathbf{Z}}$ axis and the vector from the chief to the center of the lobe. We wish to find the maximum time of flight ($\tilde{T}_{\max}$) between a starting position $\tilde{z}_o$ and final position $\tilde{z}_f$. Assume that the deputy starts and stops at the same position, then

$$\tilde{z}_f = \tilde{z}_o = \sqrt{\left(\frac{\dot{\tilde{z}}_o}{2\pi}\right)^2 + \tilde{z}_o^2}\cos\left[2\pi\tilde{T}_{\max} - \tan^{-1}\left(\frac{\dot{\tilde{z}}_o}{2\pi\tilde{z}_o}\right)\right] \tag{A4}$$

Solving for $\tilde{T}_{\max}$,

$$\cos^{-1}\left[\frac{\tilde{z}_o}{\sqrt{\left(\frac{\dot{\tilde{z}}_o}{2\pi}\right)^2 + \tilde{z}_o^2}}\right] = 2\pi\tilde{T}_{\max} - \tan^{-1}\left[\frac{\dot{\tilde{z}}_o}{2\pi\tilde{z}_o}\right]$$

$$\cos^{-1}\left[\frac{1}{\sqrt{\left(\frac{\dot{\tilde{z}}_o}{2\pi\tilde{z}_o}\right)^2 + 1}}\right] + \tan^{-1}\left[\frac{\dot{\tilde{z}}_o}{2\pi\tilde{z}_o}\right] = 2\pi\tilde{T}_{\max}$$

$$\cos^{-1}\left[\frac{1}{\sqrt{\left(\frac{\dot{\tilde{z}}_o}{2\pi\tilde{z}_o}\right)^2 + 1}}\right] + \cos^{-1}\left[\frac{1}{\sqrt{\left(\frac{\dot{\tilde{z}}_o}{2\pi\tilde{z}_o}\right)^2 + 1}}\right] = 2\pi\tilde{T}_{\max}$$

Collecting terms and substituting Eq. (A3),

$$\tilde{T}_{\max} = \frac{1}{\pi}\cos^{-1}\left[\frac{1}{\sqrt{\left(\frac{\dot{\tilde{z}}_o}{2\pi\tilde{z}_o}\right)^2 + 1}}\right] = \frac{1}{\pi}\cos^{-1}\left[\frac{1}{\sqrt{\left(\sqrt{\left(\frac{\tilde{z}_{\max}}{\tilde{z}_o}\right)^2 - 1}\right)^2 + 1}}\right] = \frac{1}{\pi}\cos^{-1}\left(\frac{\tilde{z}_o}{\tilde{z}_{\max}}\right) \tag{A5}$$

Next we find the ΔV required to stay within the $\hat{\mathbf{Z}}$ constraints. The instantaneous change in velocity at the burn points is [11]

$$\Delta\tilde{V}_Z = \dot{\tilde{z}}_i^+ - \dot{\tilde{z}}_i^- \tag{A6}$$

The relative velocity before the burn ($\dot{\tilde{z}}_i^-$) is the final relative velocity from the prior leg, and the relative velocity after the burn ($\dot{\tilde{z}}_i^+$) is the initial relative velocity of the next leg. The relative velocities are found via Eqs. (10) and (11):

$$\dot{\tilde{z}}_i^+ = \dot{\tilde{z}}_o = -2\pi z_o\frac{\cos(2\pi\tilde{T}^+)}{\sin(2\pi\tilde{T}^+)} + 2\pi\tilde{z}_f\frac{1}{\sin(2\pi\tilde{T}^+)} \tag{A7}$$

$$\dot{\tilde{z}}_i^- = \dot{\tilde{z}}_f = -2\pi\tilde{z}_o\frac{1}{\sin(2\pi\tilde{T}^-)} + 2\pi\tilde{z}_f\frac{\cos(2\pi\tilde{T}^-)}{\sin(2\pi\tilde{T}^-)} \tag{A8}$$

$\Delta\tilde{V}$ is linear in $\tilde{z}_o$ and $\tilde{z}_f$; thus, we will choose the smallest allowable $\hat{\mathbf{Z}}$ coordinate allowed by the lobe designated by $z_{\min}$. Further, assume that the period (time of flight) of the each oscillation in $\hat{\mathbf{Z}}$ is constant and designated by $\tilde{P}_z$. Thus,

$$\Delta\tilde{V}_Z = \left[-2\pi z_{\min}\frac{\cos(2\pi\tilde{P}_z)}{\sin(2\pi\tilde{P}_z)} + \frac{2\pi z_{\min}}{\sin(2\pi\tilde{P}_z)}\right] - \left[\frac{-2\pi z_{\min}}{\sin(2\pi\tilde{P}_z)} + 2\pi z_{\min}\frac{\cos(2\pi\tilde{P}_z)}{\sin(2\pi\tilde{P}_z)}\right] = 4\pi z_{\min}\left[\frac{1-\cos(2\pi\tilde{P}_z)}{\sin(2\pi\tilde{P}_z)}\right] = 4\pi z_{\min}\tan(\pi\tilde{P}_z) \tag{A9}$$

or, in terms of a specific ΔV using Eq. (20),

$$\Delta\breve{V}_Z = \Delta\tilde{V}_Z/2\pi = 2\tilde{z}_{\min}\tan(\pi\tilde{P}_z) \tag{A10}$$

Assume that the total hover time ($\tilde{T}_T$) is given and that the deputy enters the lobe with the proper entry velocity to place it on the desired oscillation (there is no entry burn). The total number of burns required to keep the deputy inside the lobe is

$$\text{no. of burns} = \lfloor\tilde{T}_T/\tilde{P}_z\rfloor \tag{A11}$$

and the ΔV required is

$$\Delta \check{V}_Z = 2\lfloor \tilde{T}_T/\tilde{P}_z \rfloor \tilde{z}_{\min} \tan(\pi \tilde{P}_z) \tag{A12}$$

Equation (38) converges to the $\hat{\mathbf{Z}}$ portion of the continuous ΔV solution [Eq. (30)] as $\tilde{P}_z$ goes to zero and is proven herein. As $\tilde{P}_z \to 0$, the small angle approximation reveals

$$\tan(\pi \tilde{P}_z) = \frac{\sin(\pi \tilde{P}_z)}{\cos(\pi \tilde{P}_z)} \approx \frac{\pi \tilde{P}_z}{1} = \pi \tilde{P}_z \tag{A13}$$

The total time of flight will be a multiple of the period of oscillation; therefore,

$$(1/k_z)\tilde{T}_T = \tilde{P}_z \tag{A14}$$

where k_z is the number of $\hat{\mathbf{Z}}$ legs (oscillations). Then,

$$\Delta \check{V}_Z = \left\lfloor \frac{\tilde{T}_T}{\frac{1}{k_z}\tilde{T}_T} \right\rfloor * 2\tilde{z}_{\min}\left(\pi \frac{1}{k_z}\tilde{T}_T\right) = 2\tilde{z}_{\min}\pi \lfloor k_z \rfloor \frac{1}{k_z}\tilde{T}_T \tag{A15}$$

Because k_z is an integer:

$$\lfloor k_z \rfloor = k_z \tag{A16}$$

Thus,

$$\Delta \check{V}_Z = 2\tilde{z}_{\min}\pi \tilde{T}_T \tag{A17}$$

which is the same as the continuous-thrust solution in Eq. (30). The constraint on choosing k_z is

$$(1/k_z)\tilde{T}_T = \tilde{P}_z \le \tilde{T}_{\max} \tag{A18}$$

Solving for k_z,

$$k_z \ge \tilde{T}_T/\tilde{T}_{\max} \tag{A19}$$

Because k_z is an integer:

$$k_z = \lceil \tilde{T}_T/\tilde{T}_{\max} \rceil \tag{A20}$$

Assuming no entry burn is required, the total number of burns required will be $k_z - 1$. Therefore, the total ΔV is

$$\Delta \check{V}_Z = 2\tilde{z}_{\min}(k_z - 1)\tan(\pi \tilde{P}_z) = 2\tilde{z}_{\min}(k_z - 1)\tan(\pi \tilde{T}_T/k_z) \tag{A21}$$

Acknowledgment

The research presented in this document is sponsored by the U.S. Air Force Research Laboratory's Space Vehicles Directorate.

References

[1] Broschart, S. B., and Scheeres, D. J., "Control of Hovering Spacecraft Near Small Bodies: Application to Asteroid 25143 Itokawa," *Journal of Guidance, Control, and Dynamics*, Vol. 28, No. 2, March–April 2005, pp. 343–354. doi:10.2514/1.3890

[2] Hu, W., and Scheeres, D., "Spacecraft Motion About Slowly Rotating Asteroids," *Journal of Guidance, Control, and Dynamics*, Vol. 25, No. 4, July–Aug. 2002, pp. 765–775. doi:10.2514/2.4944

[3] Hope, A. S., and Trask, A. J., "Pulsed Thrust Method for Hover Formation Flying," American Astronautical Society Paper 03-655Aug. 2003.

[4] Lovell, T. A., and Brown, D. L., "Impulsive-Hover Satellite Trajectory Design for Rendezvous and Proximity Operation Missions," American Astronautical Society Paper 07-102, Feb. 2007.

[5] Vaddi, S. S., Vadali, S. R., and Alfriend, K. T., "Formation Flying: Accommodating Nonlinearity and Eccentricity Perturbations," *Journal of Guidance, Control, and Dynamics*, Vol. 26, No. 2, March–April 2003, pp. 214–223. doi:10.2514/2.5054

[6] Wiesel, W. E., *Spaceflight Dynamics*, 2nd ed., McGraw–Hill, Boston, MA, 1997, pp. 44–72.

[7] Lovell, T. A., and Tragesser, S. G., "Guidance for Relative Motion of Low Earth Orbit Spacecraft Based on Relative Orbit Elements," AIAA Paper 2004-4988, Aug. 2004.

[8] Clohessy, W., and Wiltshire, R., "Terminal Guidance System for Satellite Rendezvous," *Journal of the Aerospace Sciences*, Vol. 27, No. 9, Sept. 1960, pp. 653–659.

[9] Mullins, L. D., "Initial Value and Two Point Boundary Value Solutions to the Clohessy–Wiltshire Equations," *Journal of the Astronautical Sciences*, Vol. 40, No. 4, Oct.–Dec. 1992, pp. 487–501.

[10] Lovell, T. A., and Tollefson, M. V., "Calculation of Impulsive Hovering Trajectories via Relative Orbit Elements," American Astronautical Society Paper 05-409, Aug. 2005.

[11] Wie, B., *Space Vehicle Dynamics and Control*, 1st ed., AIAA, Reston, VA, 1998, pp. 261–303.